International Journal of Agriculture and Biosciences 2025 14(2): 209-222.
https://doi.org/10.47278/journal.ijab/2024.211

RESEARCH ARTICLE
eISSN: 2306-3599; pISSN: 2305-6622

Remote Sensing Techniques for Detecting Soil Salinization from 1985 to 2021 in Hot and Hyper-Arid Saham Basin, Oman

Yaseen Al-Mulla *,[1,2], Khalid Al-Mahrezi[3], Mohammed Al-Hammadi[4], Ahsan Ali[1] and Krishna Parimi[1]

[1]Remote Sensing and GIS Research Center, Sultan Qaboos University, Al-Khod, Muscat, Sultanate of Oman
[2]Department of Soils, Water and Agricultural Engineering, Sultan Qaboos University, Al-Khod, Muscat, Sultanate of Oman
[3]Oman Tourism Development Company, Muscat, Sultanate of Oman
[4]Abu Dhabi Agricultural & Food Safety Authority, Abu Dhabi, United Arab Emirates
*Corresponding author: yalmula@squ.edu.om

ABSTRACT

Environmental changes resulting from climatic change, freshwater scarcity, and soil-water salinization necessitate an in-depth investigation and assessment of their impacts. The impact of soil and water salinization in a hot and hyper-arid region such as Oman is more obvious in the agriculture sector, especially in the Al-Batinah coastal region of the country. This study aimed to assess, map, and track soil in the study area using remote sensing techniques. Landsat images covering 36 years were acquired along with Cartosat and WorldView-2 satellite images for accuracy assessment and validation. A satellite image-based salinity detection and delineation model was developed for the study area. The imagery was successfully classified with an overall accuracy of 80%, with supervised and unsupervised classification accuracy ranging from 76 to 84%, respectively. Spatiotemporal change detection identified that agricultural activity decreased by 30% (4.46km^2) between 1985 and 2007 compared to 17.1% (2.53km^2) between 2007 and 2021. Moreover, soil salinity has extended farther inward from the shoreline as the salinity intensity increased from 36 to 60%. These findings can be attributed to the severe effects of saltwater intrusion, which led to the abandonment/shifting of farms from the shoreline to the land/mountains, resulting in urbanization. This study calls for urgent attention and decisive action to improve area management and optimize freshwater resources in hot and hyper-arid environments.

Keywords: Change Detection, Remote Sensing, Salinization, Soil and Water, Vegetation.

Article History
Article # 24-780
Received: 24-Aug-24
Revised: 09-Dec-24
Accepted: 15-Dec-24
Online First: 27-Dec-24

INTRODUCTION

The overexploitation of coastal groundwater leads to salt accumulation in the soils (Abulibdeh et al., 2021). Soil salinity has a detrimental influence on soil's physicochemical properties, plant development and production, ecosystem biological processes, and soil and water resources (Ren et al., 2019; Wen et al., 2019; Guo et al., 2023). As salinity levels increase, plants face serious difficulties in extracting water from the soil, causing water stress conditions. Moreover, the accumulation of salts in the soil can cause plant toxicity, nutrient imbalances (Ashrafi et al., 2018), and a decrease in water infiltration rates (Jarraya & Benabdallah, 2020). Hence, soil salinity has been pointed out as one of the main factors that limited plant growth in arid and semi-arid areas (Foster et al., 2018; Abuelgasim & Ammad, 2019; Taghizadeh-Mehrjardi et al., 2021; Smanov et al., 2023). Remote sensing has repeatedly been used as a promising tool to obtain information regarding soil properties (Ben-Dor et al., 2018; Gorji et al., 2019; Suleymanov et al., 2023), land degradation processes (AbdelRahman et al., 2019; Abdelrahman, 2023) and canopy biophysical properties (Oteman et al., 2019; Neinavaz et al., 2021; Raj et al., 2021).

The precise assessment of salinization intensity, extent, and trends is important for better management of soil and water resources. The use of remote sensing tools is useful for the identification of salt distribution, the detection of its spatial and temporal changes, the prediction of further soil degradation and the selection of

Cite this Article as: Al-Mulla Y, Al-Mahrezi K, Al-Hammadi M, Ali A and Parimi K, 2025. Remote sensing techniques for detecting soil salinization from 1985 to 2021 in hot and hyper-arid Saham Basin, Oman. International Journal of Agriculture and Biosciences 14(2): 209-222. https://doi.org/10.47278/journal.ijab/2024.211

A Publication of Unique Scientific Publishers

the best remediation methods. Data from soil salinity maps generated by remote sensing were found to be in good agreement with those obtained from traditional methods that depended on laboratory chemical measurements (Goldshleger et al., 2012; Ibrahim, 2016; Khadim et al., 2019; Ren et al., 2019; Wen et al., 2019; Abulibdeh et al., 2021; Arora et al., 2021; Kurbatova et al., 2021; Prajapati et al., 2021). To use remote sensing data effectively, one must know and understand the spectral characteristics of the features under investigation. This can be accomplished through a better understanding of the behavior of different wavelength combinations on different soil salinity (Shahid et al., 2010; Al-Jubouri & Wheib, 2020). Ibrahim (2016) stated that the sodium absorption ratio (SAR) is an important factor for soil salinity mapping using satellite imagery, even at the initial salinity stages in arid and semi-arid regions. Abuelgasim & Ammad (2019) applied shortwave infrared and near-infrared imagery to map soil salinity by developing a soil salinity index model.

Using conventional remote sensing data, most researchers have focused on mapping saline areas or differentiating between saline and non-saline soils (Gorji et al. 2019; Ghazali et al., 2020). Remote sensing observations have often concentrated on severely saline soils while neglecting the slightly affected areas, which must be the target when dealing with soil degradation. Abulibdeh et al. (2021) mapped groundwater salinity by investigating 58,000 water wells categorized the salinity into five classes from high to low salinity levels, and concluded that the groundwater salinity increased relative to space and time. Ren et al. (2019) integrated soil sampling with Chinese HuanJing-1 satellite imagery and a dynamic model for analyzing the salinity level in the Hetao irrigation district, Inner Mongolia. They concluded that soil salinity depended on groundwater depth. Ashrafi et al. (2018) examined the effect of salt stress on the growth and ion accumulation of the alfalfa crop at the Isfahan University of Technology, Iran.

Zhang et al. (2011) studied the accuracy of available vegetation indices for the estimation of soil salinity and reported that the vegetation index (VI) group, which included the normalized difference vegetation index (NDVI), soil-adjusted vegetation index (SAVI), and transformed soil-adjusted vegetation index (TSAVI), was least affected by topographical factors in their study; allowing a good detection of vegetation change in large regions. Nguyen et al. (2020) assessed the soil salinity intrusion in the coastal area using Landsat 8 near-infrared bands and soil sampling techniques and utilized the SAVI, NDVI, and vegetation soil salinity index (VSSI) to perform statistical analysis of electric conductivity (EC) values from soil samples and the previously mentioned VI resulting in a strong correlation with R^2=0.89 between the soil salinity estimation using Landsat-8 satellite imagery and in situ measurement of soil salinity from soil samples. It is important to underline that when vegetation density is very low, such as in hyper-arid and arid regions, soils become the main contributing factor in the reflectance measured by the remote sensing system (Prudnikova & Savin, 2018). Thus, plant canopy reflectance strongly affects soil variation reflectance (Prudnikova et al., 2019). Huete & Jackson (1987) first indicated the influence of soil variations on spectral reflectance and found that in semi-arid and arid regions, where the vegetation cover is typically less than 30%, the NDVI values were lower at similar vegetation percentages in lighter soil than in darker soil.

Several studies have examined the performance of the above-mentioned VIs in areas with low vegetation covers. Goldshleger et al. (2012) proposed a new member for the SAVI family and introduced a generalized soil-adjusted vegetation index (GESAVI) and compared it with other VIs, including the NDVI, SAVI, perpendicular vegetation index (PVI), optimized soil-adjusted vegetation index (OSAVI), and TSAVI. They found that the GESAVI and then the SAVI and OSAVI were the most accurate VIs. Comparing several vegetation indices as a proxy to monitor soil salinity, Zhang et al. (2011) reported that most vegetation indices had weak relationships with soil salinity except the SAVI. Alamdarloo et al. (2018) calculated the temperature condition index (TCI) and the vegetation condition index (VCI) using land surface temperature (LST) (MODIS product MOD11A2 and MOD13A2) in different climatic regions of Iran. Their study stated that vegetation health is affected by the differences in climatic and topographical conditions. A study of the trend assessment of drought in Saudi Arabia was conducted using the NDVI, a rainfall dataset, and LST estimation (Hereher et al., 2022). Their study measured a decline in vegetation and an increase in LST (locally) for the study period. Al-Mulla & Al-Adawi (2009) mapped the temporal changes of soil salinity in the Al-Rumais/Barka region of Oman using Landsat satellite images of three different dates (1991, 2005, and 2007) and claimed that remote sensing techniques provided good evidence of extreme saline soil mapping.

In coastal areas around the globe, soil salinity is an augmenting issue that directly affects the natural environment and causes economic losses by directly Impacting food safety and agricultural productivity (Nguyen et al., 2020). Therefore, soil salinity monitoring is important for the efficient management of salinity-affected areas through remediation and utilization processes of the affected soil. The impact of the salinity in Oman is obvious in the agriculture sector, especially in the Al-Batinah coastal region (Abulibdeh et al., 2021), which is the main agricultural area in the country (Siebert et al., 2007). This salinity area covers an extensive region between 10 and 30km wide from the sea toward the land (Abulibdeh et al., 2021). This coastal region extends from the capital Muscat to the United Arab Emirates (UAE) border for a total distance of about 270km. Hussain et al. (2006) reported that there was no salinity issue in this region at the end of the 1970s and the issue arose in the 1980s and 1990s with the increase in agriculture and groundwater extraction. Ibnouf & Abdelmagid (1994) observed a 38% increase in the salinity level in the Batinah region. Al-Ajmi & Abdel Rahman (2001) found that excessive groundwater pumping led to seawater intrusion, resulting in an increase in soil salinity and a decrease in soil fertility.

The above studies which were carried out in Oman have shed important light on soil salinity across a broad region. However, there is a significant opportunity to delve deeper into long-term soil salinity patterns by utilizing high-resolution satellite imagery. This study provides a more comprehensive understanding of soil salinity dynamics over time, paving the way for more effective management strategies. The impact of salinity on soils and water significantly threatens agricultural production and vegetation, necessitating urgent investigation into its detection, mapping, and effects. Additionally, the above-mentioned previous studies show a clear research gap in integrating salt-affected studies in Oman with remote sensing techniques, highlighting the need for targeted research in this area. The main objective of this study was designed to (i) assess the soil salinity status in the hot and hyper-arid conditions of the Al-Batinah coastal region of Oman using in situ soil and vegetation measurements; (ii) estimate and assess soil salinity by remote sensing tools based on change detection techniques from 1985 to 2021; and (iii) spatiotemporal mapping and classification of the soil salinity of the studied area. This study shall fill a decisive gap of utilizing satellite imagery to present a comprehensive overview of the spatiotemporal changes in soil and water deterioration due to increasing salinity along the coast of Oman. The trends identified will serve as valuable tools for reclamation strategies, aiding decision-makers and policymakers in various sectors, including urban and agricultural planning.

MATERIALS & METHODS

Fig. 1 shows the flow diagram of the study design including the satellite imagery processing, vegetation change detection, soil salinity machine learning model development, classification, and construction of results using in-situ measurement from the soil sampling.

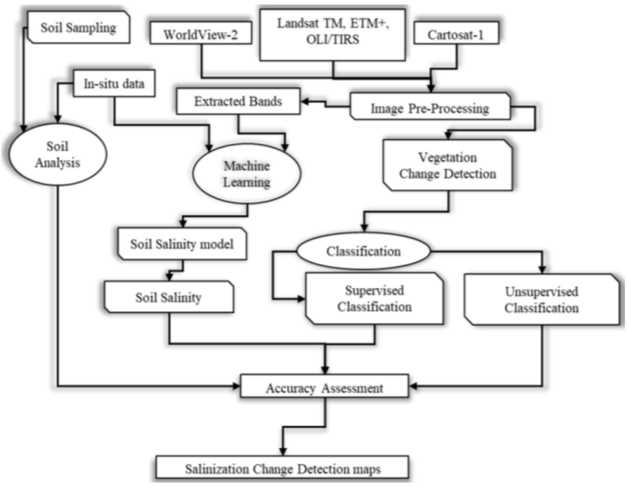

Fig. 1: Flowchart illustrating the methodology of work.

Study Area

The study area is located in the Al-Batinah region in the northern part of Oman along the coastal line 150km north of Muscat (Fig. 2). It lies between 24° 06′ 06″ north and 56° 55′ 48″ east. This study area has a hot and hyper-arid climate characterized by an average annual temperature of 26.9 °C but can reach up to 37 °C during the summer months of June and July with an average annual rainfall of 74 mm (Ali et al., 2021). The study area is mostly covered with sandy to silty clay soil (Béchennec et al., 1992; Al-Rawas et al., 2006) as it is located between the coastal plain and coastal sediments, which are linked to the geology of the north mountain ranges; tectonically placed with late Paleozoic, Mesozoic continental margin, and Tethys deep-sea sediments, as well as a slab of Cretaceous oceanic crust and mantle (Robertson et al., 1990). The Sultanate in general, including the study area, depends on groundwater from springs and wells. Aquifers are replenished by occasional rainfall while the renewable groundwater supplies are estimated at 1300 million m^3 annually (Al-Jazi & Almaany, 2020).

Soil Sampling and Analysis

Thirty soil samples were collected randomly (at a depth of 15 cm) with three replicates from each location from a 25x25m area. The latitude and longitude location of each sample (Fig. 3) were determined on the Landsat images and then followed on the ground using GPS (eTrex model from Garmin Ltd., USA). These samples were collected when the ground was covered with vegetation including halophytes. During field investigations, each sampled site was described in terms of land use, vegetation, and soil surface aspect, with particular emphasis on the surface crust. Analysis of the soil samples was conducted for the soil textural analysis by following the protocol of Beretta et al. (2014) and salinity (using JENWAY 4510), pH, and macro elements were measured by following the methods of Botero et al. (2010).

The soil water extracts were analyzed for microelements such as sodium (Na), phosphorus (K), calcium (Ca), magnesium (Mg), and chloride (Cl) using an inductively coupled plasma optical emission spectrometer (ICP-OES) in the Sultan Qaboos University. Soil texture analysis was conducted using hydrometer methods proposed by Bouyoucos, (1936) and soil class was determined with the International Soil Science Society (ISSS) triangle (Saxton et al., 1986).

Satellite Images

Five cloud-free satellite images were generated using Landsat TM at Path "159" and Row "43" (acquired on 4 February 1985), ETM+ at Path "159" and Row "43" (acquired on 3 July 2007), and OLI/TIRS at Path "159" and Row "43" (acquired 1 July 2021). The Landsat TM, ETM+, and OLI/TIRS sensors provided images with a 30-m pixel size. In addition, a stereoscopic earth observation satellite (Cartosat-1) geometrically corrected image for 2007 was provided by the Supreme Committee for Town Planning in the Sultanate of Oman. This process was repeated for the very high-resolution satellite (WorldView-2) image for the year 2021 provided by the Remote Sensing and GIS Research Center from Sultan Qaboos University, Oman. WorldView-2 was used as ancillary data for geometric correction of the Landsat images. The resolution of the Cartosat-1 image was 2.5m, while the resolution of WorldView-2 was 0.5m. The digital data processing was performed using ERDAS Imagine and ArcGIS Pro platforms.

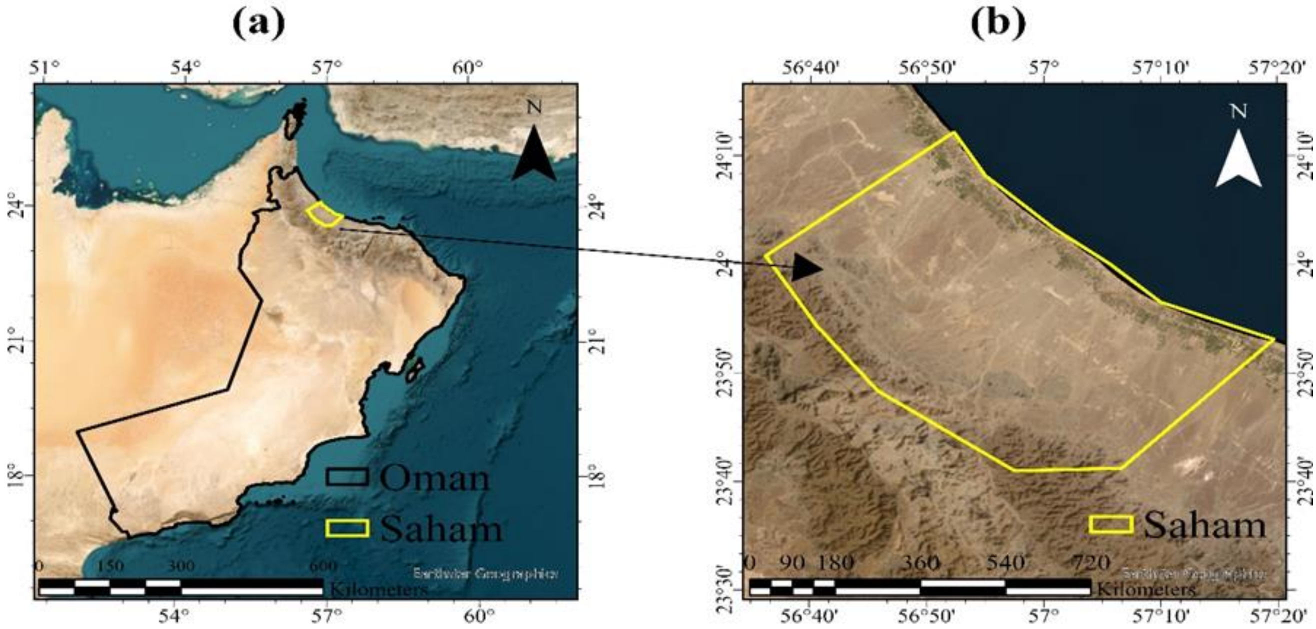

Fig. 2: Location of (b) study area in (a) Oman.

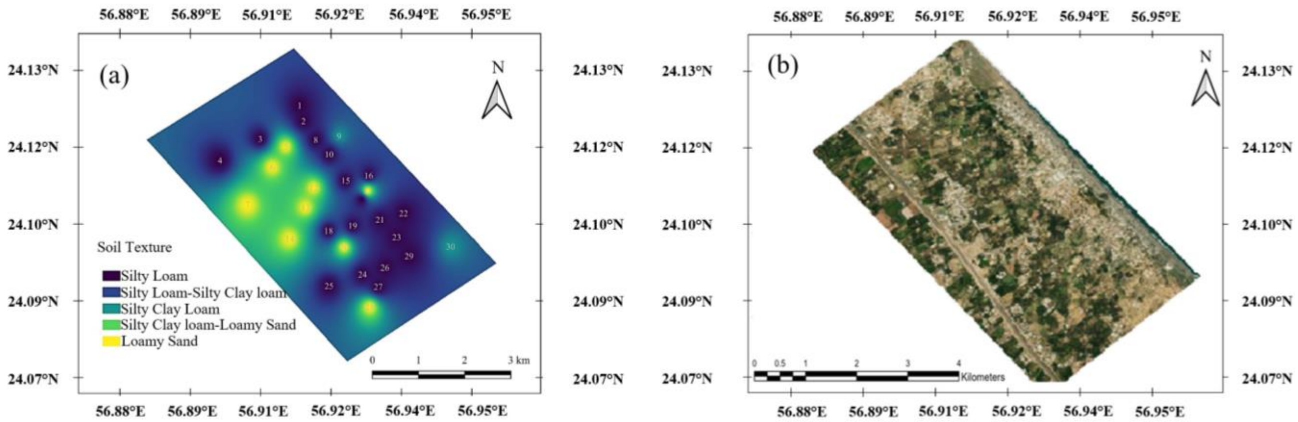

Fig. 3: The spatial distribution of the soil sample collection, numbered 1 to 30, indicating their soil texture (a) compared to the true-color composite red, green, and blue satellite image (b) of the study site.

Geometric Correction

The acquired satellite images in this study were geometrically corrected to bring them all into standard projection. Thus, it was easier to conduct a change detection process by overlaying the different year images of the same area. Moreover, the geometric correction procedure helped in overlaying the lower-resolution images on the high-resolution images for validating the unsupervised classification process. The images were rectified to the World Geodetic System (WGS 84) using zone 40 Universal Transverse Mercator (UTM) projection. After that, 13 GCPs were determined in the Cartosat and WorldView-2 images, and then errors with GCPs were reduced by moving the position of points on the images. A root means square error (RMSE) of less than 0.2 pixels was achieved in matching the ETM+ 2007 and Cartosat images as well as the OLI/TIRS and WorldView-2. Many studies claimed that multi-temporal data analysis requires accurate geometric co-registration within an accuracy of one pixel or less (Mouat et al., 1993; Chughtai et al., 2021). First-order polynomial transformation with nearest-neighbor resampling was used to resample the Landsat images to 25x25m pixel size. Nearest-neighbor resampling offers key advantages that make it an excellent choice for image processing. It effectively preserves the spectral values of the original dataset, ensuring minimal alteration of pixel brightness. This integrity is vital for reliable analyses. Additionally, its computational simplicity enhances efficiency, allowing for quicker processing without sacrificing quality. This combination of accuracy and ease of use makes it a preferred method in remote sensing applications (Campbell, 1987; Taunk et al., 2019; Bansal et al., 2022).

To perform a change analysis of vegetation, the Landsat TM image of 1985 was registered to the rectified Landsat ETM+ 2007 reference image. However, the second-order polynomial transformation was applied in the 2007 image using nearest-neighbor resampling. This was then resampled to a 25x25m pixel size. Eighteen image-to-image control points were selected and an RMSE of less than 0.2 pixels was achieved to match the Landsat TM 1985 image to the Landsat ETM+ 2007 rectified image. This procedure aimed to bring the two images to a standard projection, and they consequently fit each other.

Image Enhancement

In this study, image enhancement was performed to improve visual interpretation by increasing the distinction between healthy and unhealthy vegetation. This was achieved with spatial enhancement filtering. The Wallis Adaptive Filter (a specific filter found in ERDAS Imagine software) was used to enhance the visual appearance of the images. There are four different image enhancement functions in ERDAS Imagine. These are the Wallis Adaptive Filter, Sensor Merge, Texture Analysis, and Brightness Adjustment. The Wallis Adaptive Filter is an enhancement filter that adjusts an image based on the "contrast stretch" of the image gathered from a specific area within the image. After the Wallis Adaptive Filter enhancement was conducted it was easy to see the difference between the images.

Image Transformations

Both the NDVI and SAVI were applied in this study because these vegetation indices are highly correlated with plant water content and thus the trees' health (Al-Mulla & Al-Adawi, 2009; Zhang et al., 2011; Vani & Mandla, 2017; Nguyen et al., 2020). The two vegetation indices were calculated using ERDAS Imagine software based on Equations (1) and (2) following (Ali et al., 2021).

$$NDVI = (NIR - Red)/(NIR + Red) \tag{1}$$

$$SAVI = (L + 1)[\frac{NIR - Red}{NIR + Red + L}] \tag{2}$$

Where NIR is the near-infrared band, Red is the red band, and L is the soil brightness correction factor. The two vegetation indices were produced for the Landsat OLI/TIRS 2021, Landsat ETM+ 2007, and Landsat TM 1985. The NDVI and SAVI values were used for the visual separation of healthy and unhealthy vegetation where the values ranged between -1 (water surface) and +1 (dense green vegetation), while 0 corresponded to barren areas or soil. Since the values of L in Equation (2) differ with vegetation density from 0 for higher densities and 1 for lower densities, the SAVI was generated with a correction factor of 0.5 based on intermediate vegetation density. SAVI was later used for change detection of vegetation between 1985, 2007, and 2021. Consequently, these indices displayed healthy vegetation as bright areas with a higher value of vegetation indices and unhealthy vegetation as different dark levels of gray, which were masked out from all other terrain features.

Vegetation Change Detection Analysis Using SAVI

In change detection analysis, the main principle is that if any change in land cover occurs, it will cause a change in pixel response. The SAVI transformed images were used in detecting vegetation change in this study to minimize both soil background and atmospheric effects. Vegetation change analysis was performed as decreased, stable (no change), and increased using the SAVI images of 1985, 2007, and 2021. The dataset included both years for the SAVI. Decreased, increased, and no change threshold values in vegetation were established and applied to the SAVI dataset. The values ranged from -1.0 to 1.0; the values below 0 indicated no vegetation, and values above 0 indicated the density of the vegetation, as the SAVI uses L as the soil brightness correction factor to minimize soil brightness influences.

Images Classification

Two methods were used to classify multispectral images: unsupervised and supervised. Since supervised classification utilizes visual interpretation or relevant ground truth data as baseline data, it can usually extract more realistic information and proves to be more accurate than unsupervised classification (Ioka & Koda, 1986; Chang et al., 2020; Richards, 2022). On the other hand, unsupervised classification does not require training sites for ground truthing as a basis for classification and groups the multispectral data into several classes based on the same intrinsic similarity within each class (Chang et al., 2020; Mohammed et al., 2023). Since spectral signatures showed high variability within the classes in the study area, both methods of classification were used.

Soil Salinity Estimation using Surface Reflectance

A multitude of studies have employed satellite, UAVs, and terrestrial radiometric techniques to identify and assess soils that are affected by salinity (Fan et al., 2016; Oteman et al., 2019; Ghazali et al., 2020; Abuzaid et al., 2023). This study developed a model using an integrated approach that used satellite imagery to estimate soil salinity (Fig. 4).

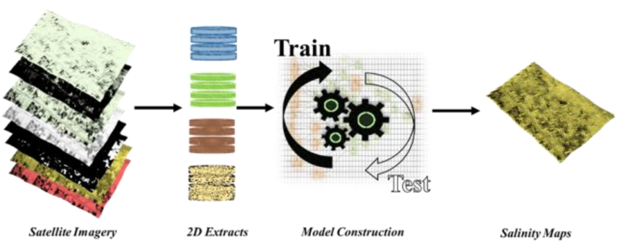

Fig. 4: Graphical layout of the integrated approach for soil salinity estimation.

The soil salinity model (equation 3) was created to estimate the soil salinity based on the spectral response of the soil to different wavelengths. To construct the model, Global Positioning Systems-based points were imported in the "ArcGIS Pro" and overlaid at the satellite imagery. Using this process, the relative pixel values were extracted using geoprocessing tools in the "ArcGIS Pro". Then the model was constructed using the "Google Colab platform". A 2D dataset was uploaded in the "Google Colab" and a total number of 70% of the data was used to train the model. Once the model was successfully trained, the model was run over the study area to create soil salinity maps.

$$SS = (\gamma_{0.45-0.52}(\omega_1)) + (\gamma_{0.52-0.60}(\omega_2)) + (\gamma_{0.63-0.69}(\omega_3)) + (\gamma_{0.77-0.0.9}(\omega_4)) + (\gamma_{1.55-1.75}(\omega_5)) + (\gamma_{2.09-2.35}(\omega_6)) - 699 \tag{3}$$

Where, γ_n is the designated band (γ) with its wavelength (n) in nm, while ω_1 = -3.495, ω_2 = 9.5756, ω_3 = 1.1744, ω_4 = 6.325, ω_5 = -2.192, and ω_6 = -1.208

Unsupervised Classification

The unsupervised classification was performed using the ISODATA algorithm within the ERDAS image-processing software package. Numerous research employed the ISODTA algorithm and reported positive outcomes in this field (King & Salem, 2012; Shahid, 2013; Lemenkova, 2021). It was performed on the images for the separation of vegetation cover existing in the study area (Vimala et al., 2020). A 95% convergence threshold was specified for the unsupervised classification of each image, and a total of 14 classes were specified in each case. This technique employed the computer-assisted formula to mathematically break up the components of the satellite data into different classes for qualitative and quantitative analysis. The maximum number of iterations used in the unsupervised classification was fixed at 25.

Ground Truthing

The main purpose of ground observation in remote sensing applications is to help establish relationships and thus to convert the digital image data from feature space into information in geographical space (Gangjun, 1996; Wu et al., 2023). The utility of remotely sensed data depends on the capability to associate spectral response patterns recorded in the data with actual environmental ground attributes. During the fieldwork for the sampling period, the observations were recorded with the coordinates of the locations of samples, and pictures were taken to give a clear image of the site and vegetation. Then, intensive field visits were made to identify the land-cover classes on the high-resolution images, supported by the unsupervised classification. The land-cover classes were revised again to ensure the categorization of the land-cover classes was correct. GPS was used to locate different land-cover classes in the high-resolution image and unsupervised classification image. These classes were used as training classes for supervised classification (Table 1).

Supervised Classification

Supervised classification generally falls into the field of statistical discriminate analysis in which training samples are extracted from known categories. Each unknown individual pixel is discriminated according to the statistical distance or similarity between the pixel and known sample clusters (Yu et al., 2019). It has been proved that the supervised classification is effective for monitoring salt buildup (Muller & van Niekerk, 2016; Fadda et al., 2019; Abulibdeh et al., 2021). By using the land-cover classes generated from ground truthing and the unsupervised classification, training regions were selected for supervised classification using the ArcGIS Pro software. On the false-color composite (FCC), the classes were identified as polygons, and the maximum likelihood classification model was chosen by assuming that histograms of the bands of data were normally distributed. The classification model used was a maximum likelihood classifier, class reparability was estimated by calculating the transformed divergence, and then thematic maps were produced.

Accuracy Assessment

Supervised classification accuracy can be evaluated through an error matrix, which is the most common procedure for expressing classification accuracy (Donoghue, 2001; Chughtai et al., 2021). The error matrix compares the classified data points to the reference ground-truthing dataset that includes the training classes. Classification accuracy assessments were created by comparing the supervised classification results with the field data. A stratified random scheme was used to identify the points for the classification accuracy assessments, where the stratification was determined by the land-cover category to ensure a representative range of test samples. The reference pixels were randomly selected by following the protocol of (Congalton, 1991). The overall percentage accuracy and the statistic kappa coefficient (K^) were calculated following the protocol of (Donoghue, 2001). The accuracy assessment was also produced for the unsupervised classification of the images by following the default procedure in the ERDAS Imagine package. Both the overall percentage accuracy and K^ were calculated.

RESULTS

Soil Analysis

The analysis of soil samples from the 30 sites within the study area revealed a constructive range of textures, from silty loams to silty clay (Fig. 3a). Notably, 28 of the samples demonstrated salinity levels above 4 dS m^{-1}, while only 2 samples fell below this threshold, highlighting the prevalence of saline soils that provides an opportunity for targeted management strategies. The EC values ranged from 1.1 to 187.6dS m^{-1}, with a mean of 67.5dS m^{-1}, and pH values varied between 7.1 and 8.5 (Fig. 5). Salinity levels were observed to increase closer to the coastline of the Oman Sea, which indicates a need for coastal management practices. Conversely, further inland—especially in residential and non-cultivated areas—salinity levels decreased significantly due to the absence of irrigation practices. This presents an opportunity to explore sustainable land-use approaches to enhance soil health in

Table 1: Land-cover classes used in fieldwork and earth observation data analysis in the study area.

Land cover	Description
Healthy vegetation	Healthy date palm trees, lime trees, mango trees, bananas, fodders such as alfalfa and Rhodes grass, and other trees, with some contribution from (*Prosopis Juliflora*) plants.
Weak, unhealthy crops	Unhealthy date palm trees, lime trees, fodders such as alfalfa and Rhodes grass, and different types of halophytes and shrubs
Weak, scattered trees	Prosopis trees and acacia plants, very weak, unproductive date palm trees, and scattered bushes.
Urban	One/two-floor houses. White or beige colors and flat roofs.
Sand	Mainly coastal sand and asphalted roads.
Bare soil and scattered vegetation	Bare soils with few bushes and cutting grass areas.
Bare soil	Bare soils with few acacia plants and shrubs.
Bare soil with bushes	Dark color reflectance soil with bushes.
High saline soil	High saline soils with salt crust in some areas, halophytes, soil with high gravel contents, and large, white-roofed buildings.

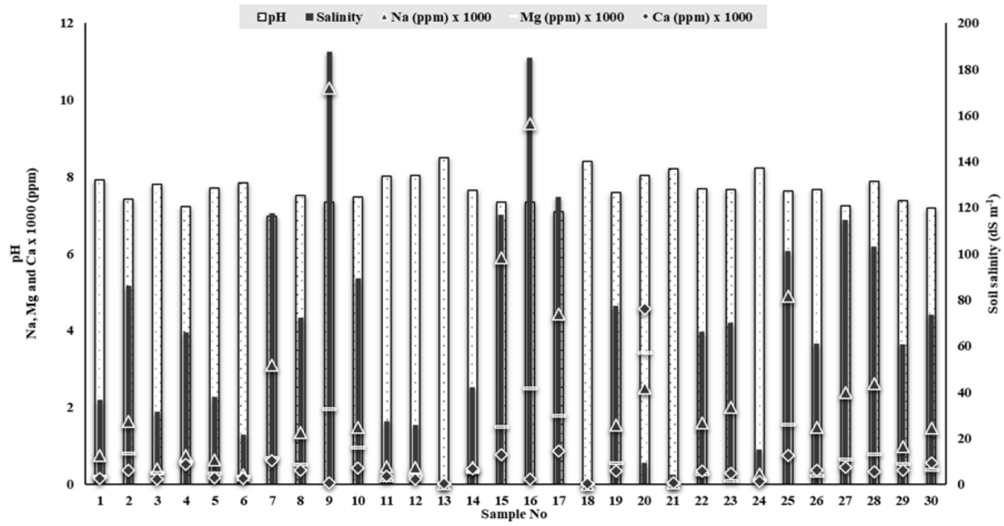

Fig. 5: Soil sample analysis results in the study area. Where salinity is in dS m^{-1} while Na, Mg, and Ca are in (value ×1000) ppm,

those areas. The salinity levels increased in the cultivated areas where intensive agriculture activities took place because seawater intrusion increased salinity owing to the excessive groundwater extraction using wells mostly installed along the coastline (Abulibdeh et al., 2021).

Vegetation Spectral Characteristics

Spectral response signatures of visible red and near-infrared wavelengths for different plants and soil types in the study area were useful for distinguishing the response of a stressed plant canopy from that of an unaffected canopy. Stressed vegetation was identified by an increase in the visible red wavelength and a decrease in the near-infrared. This could be due to a lack of pigments and the weakening of the cellular structure. The amount of green vegetation was found to be related to red absorption, which linearly decreases with increasing green vegetation. That is the basis of many vegetation indices such as the NDVI. Based on analysis, the mean difference between the SAVI values for both months (February and July) of the same year (2021) was within a range of 0.01 (Table 2). Moreover, the coefficients of variation for SAVI in February and July (in 2021) were 57 and 50, respectively. Hence, no substantial differences in the spectral signatures were found regardless of the month considered (i.e., images acquired in February and July). This might be because most of the vegetation and crops in the area are perennial.

Table 2: Statistics of preliminary analysis of SAVI values for both months (February and July) of the same year (2021) over the study area.

Month	Mean	Median	Standard Deviation	Coefficient of Variation (%)
February, 2021	0.21	0.18	0.12	57
July, 2021	0.22	0.19	0.11	50

The results (Fig. 6a) indicated that the 1985 image was characterized by lower reflectance in the visible red and higher reflectance in the near-infrared, compared to the other two images, especially in the old, cultivated area, which is closer to the Oman Sea coast, indicating a better green vegetation cover in 1985. Soils have higher spectral reflectance in visible red as compared with the surrounding vegetation. High saline soil, bare soil, bare soil with scattered vegetation, and bare soil with bushes are shown as different levels of bright colors in the images (Fig. 6a-c). These classes had much higher spectral reflectance in visible red and near-infrared wavelengths than the sandy soils. A comparison of 1985, 2007, and 2021 images proved that the vegetation conditions in 1985 were much better than in 2007, and vegetation conditions in 2007 were better than in 2021.

Vegetation Indices

NDVI and SAVI, as spectral reflectance rationing models, were useful in enhancing the fine spectral variations that were difficult to detect on the original images. They were also effective in differentiating between healthy and unhealthy vegetation. NDVI transformation separated the soil and vegetation surfaces according to their visible red and near-infrared (NIR) contrast. SAVI transformation performed the same process by taking a soil contribution into account using the L factor. Healthy vegetation displayed a light color in both SAVI and NDVI images (higher vegetation indices values), stressed unhealthy vegetation corresponded to a gray color (lower vegetation indices values), and no vegetation exhibited black color (lowest vegetation indices values). Because no significant differences between NDVI and SAVI images were noticed (Fig. 6d) in this study, only SAVI images for all years were used (Fig. 6a-c).

Soil Salinity Maps

Spectral analysis was utilized in this work to estimate the temporal and geographical maps of soil salinity. Numerous sites within the research area were geotagged, and the soil salinity was determined using these geotagged locations. The spectral response of the saline soil was considered to construct the soil salinity model using these salinity values. The spatiotemporal changes in the study region between 2007 and 2021 are depicted in Fig. 7. In the year 2021, soil salinity levels were uniformly distributed throughout the research area, accounting for about 40% of the total land. Fig. 7(a) illustrates that in the year 2007 soil salinity values were quite high, spread from North-West to South-East with the highest salinity along the seashore. The findings from the soil salinity maps reveal a significant increase in soil salinity over time.

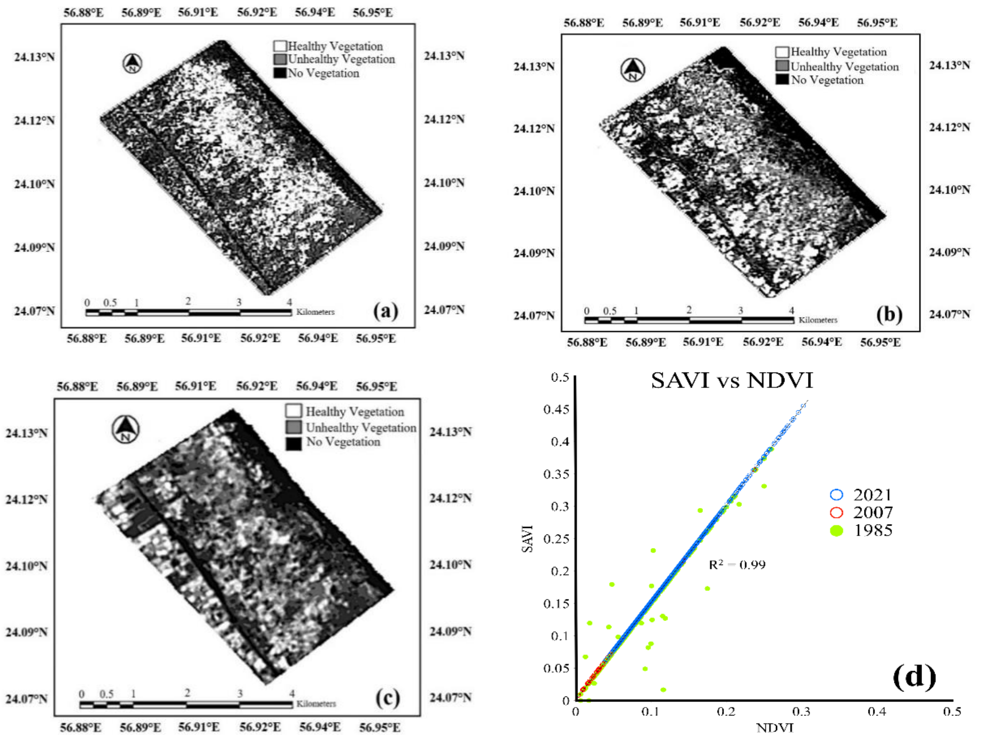

Fig. 6: Soil-adjusted vegetation index (SAVI) images of (a) 1985, (b) 2007, and (c) 2021 for the study area and (d) 1 vs 1 graph between the SAVI and NDVI in the study period.

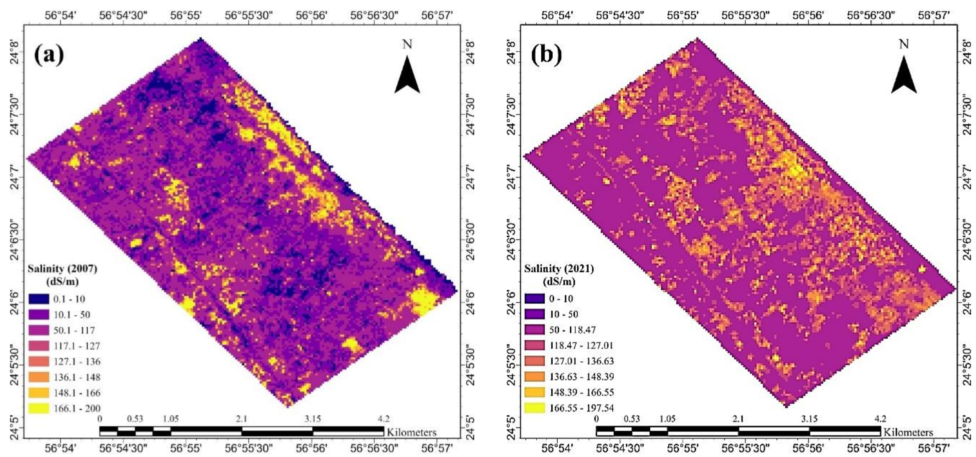

Fig. 7: Spatiotemporal distribution of the soil salinity estimated using the developed model for the years (a) 2007 and (b) 2021. Here salinity is in dS m^{-1}.

In 2007, approximately 35% of the land exhibited salinity levels classified as low to medium. However, by 2021, the situation had changed dramatically, with maps indicating that 63% of the region now fell within medium salinity levels, and 60% of the land displayed high to severe salt concentrations. Notably, 14% of the area had high salinity levels, primarily concentrated near the coastline.

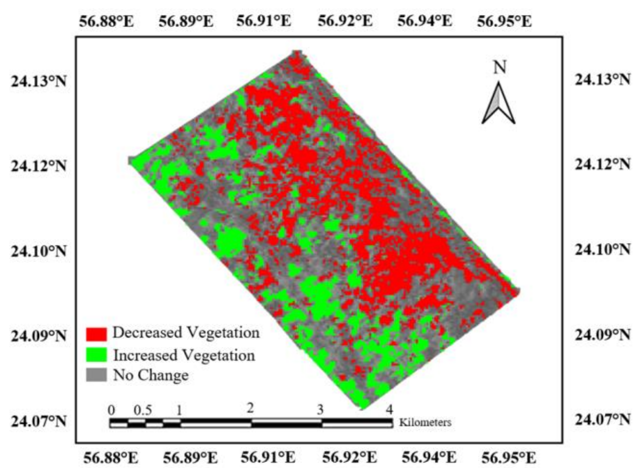

Fig. 8: Overall changes of vegetation in the study area.

Vegetation Change Detection Analysis

The change detection analysis (Fig. 8) was produced using SAVI images with a 10% threshold from 1985 to 2007 and from 2007 to 2021. Since there was no quantitative ground truth data available in 1985, the qualitative assessment of the changes in vegetation was based only on visual interpretation of the change in the image using image spatial distribution. Results showed that the 10% SAVI decrease in the vegetation of the study area from 1985 to 2007 was estimated to be about 30.0% (4.46km^2), representing a decrease in the agricultural area (i.e., stressed agriculture), while the increase was 23.8% (3.53km^2), representing an increase in the agricultural area. At the same time, about 46.2% (6.86km^2) of the agricultural area did not change during this period. On the other hand, the 10% SAVI decrease in the vegetation of the study area from 2007 to 2021 was evaluated at 17.1% (2.53km^2) while the increase was 24.1% (3.57km^2). For this period, about 58.9% of the studied area (8.75km^2) did not change its vegetation.

Classification

From the unsupervised classification of the images, up to 14 training classes were produced (Fig. 9). Comparisons were made among the spatial distributions of each class for the images, and the spatial distribution of land cover was marked as a polygon on the high-resolution images. These classes were then labeled using high-resolution images along with field observations. The old urban area that contributed to the sand training class appeared in the 1985 unsupervised classification image (Fig. 9a), but it was in neither the 2007 (Fig. 9b) nor the 2021 (Fig. 9c) image. The roofs of old residential buildings were made of asbestos with a color like sand. For that reason, these residential areas appeared like sand in the 1985 unsupervised classification image (Fig. 9a). These buildings, however, did not exist in recent years, and so they were not detected in the 2007 and 2021 images. On the other hand, stressed and scattered trees within the halophytes category and moderately saline soil category, which appeared in the 2007 unsupervised classification image, did not appear in the 1985 image since there was no significant salinity stress in that year.

Cutting Rhodes grass and shrubs, along with stressed and scattered trees such as halophytes, Prosopis, and Acacia, were challenging to distinguish in both images. This difficulty arose because cutting Rhodes grass blended into the soil background, while the grown Rhodes grass displayed a light color associated with high vegetation index values. Additionally, distinguishing between bare soil mixed with scattered vegetation and bare soil with bushes proved to be problematic. Moreover, light-colored bare soil and moderately saline soil also presented challenges in classification. These difficulties stem from various factors, including the low resolution of the images, the presence of mixed types of cultivation, and the reflectance characteristics of halophytes. The category of soil with sand was a highly affected area. This category increased along the coastal line in the 2007 image, and high soil salinity measurements were found in this area. This category contained features that could not be differentiated because of low resolution. The spectral properties classified automatically did not consistently align with the physical characteristics required for accurate mapping. After establishing the ground-truthing and training sites, we produced up to nine classes of supervised classification images for the years 2007 and 2021, as illustrated in Fig. 10. Because of the lack of high-resolution images and no ground-truth data, imagery from the year 1985 could not be used.

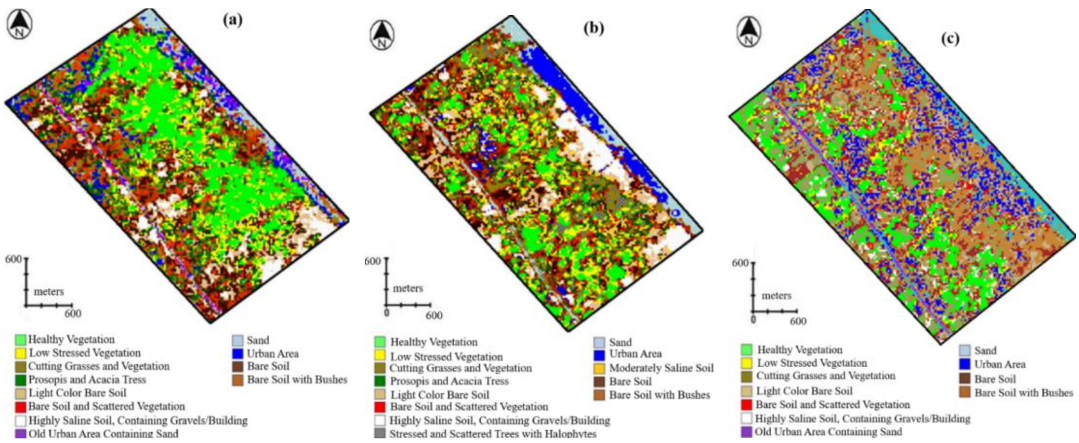

Fig. 9: Unsupervised classification of (a) 1985, (b) 2007, and (c) 2021 for the study area.

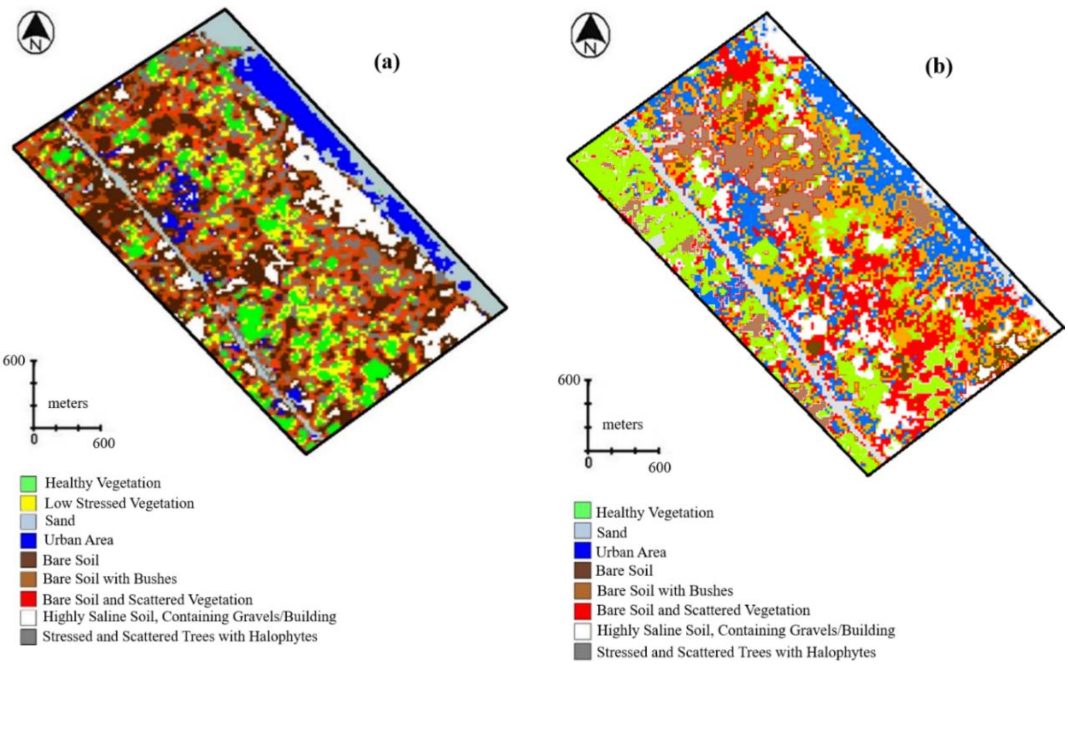

Fig. 10: Supervised classification of (a) 2007 and (b) 2021 for the study area.

When comparing the classification results to the ground truth data and Cartosat images, most classes aligned well with the reference sites. However, certain areas proved challenging to match due to confusion arising from traditional mixed agricultural practices, where forages were often interspersed among date palm trees. The lower resolution of the Landsat ETM+ image further exacerbated this confusion. Nonetheless, low-stress and stressed vegetation, as well as scattered trees in halophyte regions, were more clearly distinguishable from other types of vegetation cover. Clear detection of stressed trees was difficult and complicated by low-resolution satellite data, which may have been related to the satellite's position at space altitude and the ground cover characteristics (Diner et al., 1999). Pixel value heterogeneity was present within an individual land cover, so the selection of accurate pixels was difficult and time-consuming. One or all of these factors can alter the image-based reflectance of a canopy. Despite all the limitations mentioned above, classification was performed successfully, resulting in the delineation of most of the land-cover classes.

Accuracy Assessment

The accuracy of the unsupervised and supervised classifications was assessed by an error matrix. The overall accuracy of unsupervised classifications ranged from 76% to 84% with the kappa statistics coefficient ranging from 0.74 to 0.82. The results (Table 3) also showed that supervised classifications had an overall accuracy of 80% and a K^ value of 0.77.

Table 3: The overall accuracy (%) and Kappa Coefficient (K^) for Supervised and Unsupervised classification of Landsat TM 1985 and Landsat ETM+ 2007 images.

Classification	Classification Accuracy (%)	Kappa Coefficient (-)
Supervised Classification	80 (2007)	0.77 (2007)
Unsupervised Classification (2007)	76	0.74
Unsupervised Classification (1985)	84	0.82

DISCUSSION

Spectral response signatures of visible red and near-infrared wavelengths helped distinguish between stressed and unaffected plant canopies (Davis et al., 2023; Morales-Gallegos et al., 2023). Stressed vegetation showed an increase in visible red wavelength and a decrease in near-infrared, likely due to a lack of pigments and weakened cellular structure. The relationship between green vegetation and red absorption, which decreases linearly as green vegetation increases, forms the basis for vegetation indices like NDVI and SAVI. The use of both the NDVI and SAVI in this study is crucial due to their strong correlation with plant water content, a key factor in tree health (Zhou et al., 2022; Morales-Gallegos et al., 2023). These indices provide vital insights into plant vitality, differentiating between healthy and stressed vegetation. This dual approach enhanced our assessments of salinity's impact on vegetation health in the Al-Batinah coastal region, fostering a deeper understanding of environmental effects and aiding in the development of effective management strategies. The vegetation index images provide a detailed depiction of a notable shift in agricultural areas, highlighting a movement toward the mountainous regions and away from the coastline of the Oman Sea. In the images from 1985 (Fig. 6a), we observe that the areas with the highest SAVI values, which reflect dense and healthy vegetation, were predominantly located close to the Oman Sea. However, by 2007 (Fig. 6b), a noticeable trend emerged where these higher SAVI values began to retreat from the coastline, indicating a change in land use or agricultural practices. By the year 2021 (Fig. 6c), this trend became more pronounced, as the regions with healthy vegetation were found much farther inland, demonstrating a significant transformation in agricultural practices and land utilization over the decades. The same trend was observed in many studies (Barwani & Helmi, 2006; Al-Mulla & Al-Adawi, 2009; Asma et al., 2019; Abulibdeh et al., 2021) claiming that the salinity level increased and spread inward from the coastal line in the same period. This shift may reflect various factors, including soil salinization, climate change, urbanization, or changes in farming techniques, emphasizing the evolving relationship between agriculture and environmental conditions in this region. The findings from the salinity results (Fig. 5) obtained in the research indicated the same trend: soil salinity has extended farther inward from the shoreline as the region with salinity grew from 36% to 60% in the analyzed area. Thus, it is confirmed that the agricultural area has shifted away from the Oman Sea coastline over 36 years.

This can be further explained by the availability of fresh water in the inland direction and by the variations in soil and water salinity, which increased continuously because of the over-pumping of groundwater that allowed the seawater intrusion phenomena to occur, as addressed by Food and Agriculture Organization of the United Nations (2009), Naifer et al. (2011) and Abulibdeh et al. (2021). Many studies also claimed that the irrigation water in the studied area had high salt levels (Al-Busaidi et al., 2022; Hereher & El-Kenawy, 2022). Vegetation change detection analysis suggested that the decline in agricultural activities was greater from 1985 to 2007 than from 2007 to 2021. There was a severe effect of seawater intrusion from 1985-2007, causing the abandoning/shifting of the farms from near the coastline inland, and most of the abandoned/shifted farms near the coastline were urbanized from 2007 to 2021. The results from Deadman et al. (2016) and Al-Aufi et al. (2020) observed the same trend in the Al-Batinah region. The study compellingly demonstrates a marked decline in agricultural activities over the examined period. The findings from the SAVI change detection analysis suggest that variations in the agricultural landscape are not solely the result of increases or decreases in farming areas. Other contributing factors may also play a role in the noted changes. Notably, in certain regions, vegetation has increased due to the introduction of invasive species like *Prosopis juliflora* and various halophytes. This particular species presents a serious threat to local biodiversity, as it grows more rapidly and adapts more effectively to drought conditions than native plants, thereby undermining the ecological balance and the survival of indigenous flora (Dohai, 2007; Byalt & Korshunov, 2021; Hussain et al., 2021).

The classification results compared to the ground truth data and Cartosat images highlight a significant achievement, as most classes were closely aligned with the ground truth sites. However, it is important to note that discrepancies in certain regions arose due to the complexities of traditional mixed agricultural practices, particularly where forages are often interspersed among date palm trees. The low resolution of the Landsat ETM+ image also contributed to this confusion. The results of the interviews with the farmers indicated that the old, experienced farmers lost their agricultural land because they were no longer productive. These interviews helped understand the economic impact on farmers as incomes were very low or in some cases nonexistent from agricultural activities affected by soil salinity. These economic and environmental impacts also supported the findings by Al Jabri et al. (2019) for restrictions on farmers' good living conditions. Agricultural areas with excellent production conditions were located further inland and primarily managed by new farmers who lacked sufficient experience. This situation led to a concerning trend where the most productive lands were rented out to foreign laborers who often relied on intensive farming practices. These practices disrupt proper land rotation and result in harmful accumulations of chemical fertilizers and pesticides. Moreover, the excessive use of flood irrigation systems is depleting groundwater resources and undermining land productivity as Alqasemi et al. (2021) claimed that 66 % of the farms were using flood irrigation techniques. It is crucial to address these issues by implementing sustainable farming techniques, promoting education for inexperienced farmers, and adopting efficient water management strategies to ensure the long-term health and productivity of our agricultural lands. Immediate action is necessary to rectify these practices and safeguard the environment. Some new farmers had commercialized their farms to grow cash crops such as Rhodes grass, which needed higher amounts of water.

The salinity problems impacted the salt-affected areas environmentally, reducing plant quality and productivity. The relocation of the farms away from the coastal area also caused a reduction in fruit trees, strengthening the claim in a study by Al-Aufi et al., (2020) linking the impact of soil salinity. The impact of salinity on biological diversity also includes the limitation of native plant distribution and the promotion of exotic invasive plant species such as *Prosopis juliflora,* which can tolerate harsh saline conditions and occupy native plant species areas (Byalt & Korshunov, 2021; Hussain et al., 2021). Furthermore, the current study's findings are consistent with those of Ahmed & Askri, (2016) claiming that the rapid increase in agricultural activities in the Sultanate of Oman, as well as the over-pumping of fresh groundwater over the last three decades, has necessitated the need for comprehensive water use policies and total water resource management in Oman, particularly in Al-Batinah region.

Conclusion

This study was conducted in hot and hyper-arid conditions of Al-Batinah, in the northern coastal area of the Sultanate of Oman, and detected high soil salinity levels near sea and irrigated regions. The change detection technique provided valuable results in monitoring the decrease, increase, and stability of the green cover at a regional level. The old urban area contributing to the sand training class appeared in the 1985 unsupervised classification image but was in neither the 2007 nor the 2021 classification. These results indicated that the decline in agricultural activities was greater from 1985 to 2007 than from 2007 to 2021. The seawater intrusion was severe from 1985-2007, causing an abandoning/shifting of the farms from near the coastline inland, and most of the abandoned/shifted farms near the coastline became urbanized from 2007 to 2021. Moreover, it was observed that agricultural activities declined in the studied period. The results of this study provide compelling evidence of declining agricultural production and elevated soil salinity levels. These findings unequivocally demonstrate the urgent need to address soil and water deterioration in the region through enhanced remote sensing studies. It is imperative to develop a comprehensive water well census and implement a robust system for water extraction concessions. Employing advanced technologies, particularly remote sensing data, is essential for effectively monitoring changes in the region at various resolution levels. Additionally, a collaborative effort among governmental organizations to establish an agricultural database is crucial. Furthermore, extensive reclamation and water resource management studies must be conducted to decisively reduce the environmental and social impacts of salinity. Modern cultivation systems such as hydroponic (soilless cultivation) systems in greenhouses and modern irrigation systems should be subsidized more in the Al-Batinah region to reduce water consumption and increase the efficiency of water use. In addition, new salt-tolerant fodders should be introduced to the region.

Conflict of Interest: All authors declare no conflict of interest.

Author Contributions: Yaseen Al-Mulla: Conceptualization, Writing – review and editing, Writing – original draft, Data curation, Formal analysis, Methodology, Software, Validation: Visualization. Khalid Al-Mahrezi: Conceptualization, Writing – review and editing, Writing – original draft, Data curation, Formal analysis, Methodology, Software, Validation: Visualization. Mohammed Al-Hammadi: Conceptualization, Writing – review and editing, Writing – original draft, Data curation, Formal analysis, Methodology, Software, Validation: Visualization. Ahsan Ali: Conceptualization, Writing – review and editing, Writing – original draft, Data curation, Formal analysis, Methodology, Software, Validation: Visualization. Krishna Parimi: Conceptualization, Writing – review and editing, Writing – original draft, Data curation, Formal analysis, Methodology, Software, Validation: Visualization.

REFERENCES

AbdelRahman, M.A. (2023). An overview of land degradation, desertification and sustainable land management using GIS and remote sensing applications. *Rendiconti Lincei. Scienze Fisiche e Naturali*, *34*(3), 767-808. https://doi.org/10.1007/s12210-023-01155-3

Abdelrahman, M.A.E., Natarajan, A., Hegde, R., & Prakash, S.S. (2019). Assessment of land degradation using comprehensive geostatistical approach and remote sensing data in GIS-model builder. *Egyptian Journal of Remote Sensing and Space Sciences*, *22*(3), 323–334. https://doi.org/10.1016/j.ejrs.2018.03.002

Abuelgasim, A., & Ammad, R. (2019). Mapping soil salinity in arid and semi-arid regions using Landsat 8 OLI satellite data. *Remote Sensing Applications Society and Environment*, *13*, 415–425. https://doi.org/10.1016/j.rsase.2018.12.010

Abulibdeh, A., Al-Awadhi, T., Al Nasiri, N., Al-Buloshi, A., & Abdelghani, M. (2021). Spatiotemporal mapping of groundwater salinity in Al-Batinah, Oman. *Groundwater for Sustainable Development*, *12*(51), 100551. https://doi.org/10.1016/j.gsd.2021.100551

Abuzaid, A.S., El-Komy, M.S., Shokr, M.S., El Baroudy, A.A., Mohamed, E.S., Rebouh, N.Y., & Abdel-Hai, M.S. (2023). Predicting dynamics of soil salinity and sodicity using remote sensing techniques: A landscape-scale assessment in northeastern Egypt. *Sustainability*, *15*(12), 9440. https://doi.org/10.3390/su15129440

Ahmed, A.T., & Askri, B. (2016). Seawater intrusion impacts the water quality of the groundwater on the northwest coast of Oman. *Water Environment Research: A Research Publication of the Water Environment Federation*, *88*(8), 732–740. https://doi.org/10.2175/106143016X14609975747045

Al Jabri, S.A., Zekri, S., Zarzo, D., & Ahmed, M. (2019). Comparative analysis of economic and institutional aspects of desalination for agriculture in the Sultanate of Oman and Spain. *Desalination and Water Treatment*, *156*, 1–6. https://doi.org/10.5004/dwt.2019.24066

Al-Ajmi, H.A., & Abdel Rahman, H.A. (2001). Water management intricacies in the Sultanate of OmanThe augmentation—conservation conundrum. *Water International*, *26*(1), 68–79. https://doi.org/10.1080/02508060108686887

Alamdarloo, E.H., Manesh, M.B., & Khosravi, H. (2018). Probability assessment of vegetation vulnerability to drought based on remote sensing data. *Environmental Monitoring and Assessment*, *190*(12), 702-709 https://doi.org/10.1007/s10661-018-7089-1

Al-Aufi, K., Al-Wardy, M., Choudri, B.S., & Ahmed, M. (2020). Analysis of crops cultivation trend: a shifting scenario in a coastal Wilayat, Oman. *Environment Development and Sustainability*, *22*(3), 2685–2698. https://doi.org/10.1007/s10668-019-00309-4

Al-Busaidi, W., Janke, R., Menezes-Blackburn, D., & Mumatz Khan, M. (2022). Impact of long-term agricultural farming on soil and water chemical properties: A case study from Al-Batinah regions (Oman). *Journal of the Saudi Society of Agricultural Sciences*, *21*(6), 397–403. https://doi.org/10.1016/j.jssas.2021.11.002

Ali, A., Al-Mulla, Y.A., Charabi, Y., Al-Rawas, G., & Al-Wardy, M. (2021). Satellite-based water and energy balance model for the arid region to determine evapotranspiration: Development and application. *Sustainability*, *13*(23), 13111. https://doi.org/10.3390/su132313111

Al-Jazi, M.A.H., & Almaany, A.R. (2020). Power elements of the Sultanate of Oman during the second half of the twentieth century. *PalArch's Journal of Archaeology of Egypt/Egyptology*, *17*(6), 15243–15278. https://archives.palarch.nl/index.php/jae/article/view/6092

Al-Jubouri, A.K., & Wheib, K.A. (2020). Effect of soil salinity on the spectral reflectance of red and NIR wavelengths in the al-salamiyat project. *Plant Archive*, *20*, 1359–1365.

Al-Mulla, Y.A., & Al-Adawi, S. (2009). Mapping temporal changes of soil salinity in the Al-Rumais region of Oman using geographic information system and remote sensing techniques. In *American Society of Agricultural and Biological Engineers (ASABE) Annual International Meeting. Paper No. 095777*, Reno, NV, USA.

Al-Rawas, A.A., Goosen, M.F., & Al-Rawas, G.A. (2006). Geology, classification, and distribution of expansive soils and rocks: a case study from the Arabian Gulf. In *Expansive Soils* (pp. 15-26). CRC Press, Florida, United States.

Alqasemi, A.S., Ibrahim, M., Fadhil Al-Quraishi, A.M., Saibi, H., Al-Fugara, A.K., & Kaplan, G. (2021). Detection and modeling of soil salinity variations in arid lands using remote sensing data. *Open Geosciences*, *13*(1), 443-453.

Arora, A., Arabameri, A., Pandey, M., Siddiqui, M.A., Shukla, U.K., Bui, D.T., Mishra, V.N., & Bhardwaj, A. (2021). Optimization of state-of-the-art fuzzy-metaheuristic ANFIS-based machine learning models for flood susceptibility prediction mapping in the Middle Ganga Plain, India. *The Science of the Total Environment*, *750*, 141565. https://doi.org/10.1016/j.scitotenv.2020.141565

Ashrafi, E., Razmjoo, J., & Zahedi, M. (2018). Effect of salt stress on Growth and Ion accumulation of alfalfa (Medicago sativa L.) cultivars. *Journal of Plant Nutrition*, *41*(7), 818–831. https://doi.org/10.1080/01904167.2018.1426017

Asma, M., Abdulrahim, M., Al-Ismaili, A.K., & Al-Maktoumi, Y. (2019). Spatio-temporal distribution of greenhouses and affecting driving factors in Al-Batinah South, Oman, using GIS mapping. *American-Eurasian Journal of Sustainable Agriculture*, *13*(2), 13–33.

Bansal, M., Goyal, A., & Choudhary, A. (2022). A comparative analysis of K-Nearest Neighbor, Genetic, Support Vector Machine, Decision Tree, and Long Short Term Memory algorithms in machine learning. *Decision Analytics Journal*, *3*, 100071. https://doi.org/10.1016/j.dajour.2022.100071

Barwani, A., & Helmi, A. (2006). Sea water intrusion in a coastal aquifer: a case study for the area between Seeb and Suwaiq, Sultanate of Oman. *Journal of Agricultural and Marine Sciences*, *11*, 55–69.

Béchennec, F., Roger, J., Le Métour, J., & Wyns, R. (1992). Geological Map of Seeb, Sheet NF 40-03, Scale 1:250,000, with Explanatory Notes: Directorate General of Minerals. In *Ministry of Petroleum and Minerals*. Oman.

Ben-Dor, E., Chabrillat, S., & Demattê, J.A. (2018). *Characterization of soil properties using reflectance spectroscopy. In Fundamentals, Sensor Systems, Spectral Libraries, and Data Mining for Vegetation* (pp. 187–247). CRC press, Florida, United States.

Beretta, A.N., Silbermann, A.V., Paladino, L., Torres, D., Kassahun, D., Musselli, R., & Lamohte, A.G. (2014). Soil texture analyses using a hydrometer: modification of the Bouyoucos method. *Ciencia e Investigacion Agraria*, *41*(2), 263–271. https://dialnet.unirioja.es/servlet/articulo?codigo=5316082

Botero, W.G., de Oliveira, L.C., Rocha, J.C., Rosa, A.H., & Dos Santos, A. (2010). Peat humic substances enriched with nutrients for agricultural applications: competition between nutrients and non-essential metals present in tropical soils. *Journal of Hazardous Materials*, *177*(3), 307–311. https://doi.org/10.1016/j.jhazmat.2009.12.033

Bouyoucos, G.J. (1936). Directions for making mechanical analyses of soils by the hydrometer method. *Soil Science*, *42*(3), 225–230. https://doi.org/10.1097/00010694-193609000-00007

Byalt, V.V., & Korshunov, M.V. (2021). Distribution of invasive species Prosopis juliflora (Mimosaceae) in Fujairah (UAE). *Russian Journal of Biological Invasions*, *12*(2), 157–166. https://doi.org/10.1134/s2075111721020053

Campbell, J.B. (1987). Introduction to remote sensing. *Geocarto International*, *2*(4), 64–64. https://doi.org/10.1080/10106048709354126

Chang, Z., Du, Z., Zhang, F., Huang, F., Chen, J., Li, W., & Guo, Z. (2020). Landslide susceptibility prediction based on remote sensing images and GIS: Comparisons of supervised and unsupervised machine learning models. *Remote Sensing*, *12*(3), 502-509. https://doi.org/10.3390/rs12030502

Chughtai, A.H., Abbasi, H., & Karas, I.R. (2021). A review on change detection method and accuracy assessment for land use land cover. *Remote Sensing Applications Society and Environment*, *22*(48), 100482. https://doi.org/10.1016/j.rsase.2021.100482

Congalton, R.G. (1991). A review of assessing the accuracy of classifications of remotely sensed data. *Remote Sensing of Environment*, *37*(1), 35–46. https://doi.org/10.1016/0034-4257(91)90048-b

Davis, Z., Nesbitt, L., Guhn, M., & van den Bosch, M. (2023). Assessing changes in urban vegetation using the Normalised Difference Vegetation Index (NDVI) for epidemiological studies. *Urban Forestry & Urban Greening*, *88*(80), 128080. https://doi.org/10.1016/j.ufug.2023.128080

Deadman, M. L., Al-Sadi, A.M., Al-Wardi, M.M., Al-Kiyumi, K. S.M., Deadman, W.M., & Al Said, F.A. (2016). Spatio-temporal dynamics of land use changes in response to external pressures in Oman: Greenhouse cropping as an example. *Journal of Agricultural and Marine Sciences*, *21*, 33-45. https://doi.org/10.24200/jams.vol21iss0pp33-46

Diner, D.J., Asner, G.P., Davies, R., Knyazikhin, Y., Muller, J.-P., Nolin, A.W., Pinty, B., Schaaf, C.B., & Stroeve, J. (1999). New directions in earth observing: Scientific applications of Multiangle remote sensing. *Bulletin of the American Meteorological Society*, *80*(11), 2209–2228. https://doi.org/10.1175/1520-0477(1999)080<2209:ndieos>2.0.co;2

Dohai, B.S. (2007). *Modeling of invasive exotic plant dynamics in arid region using remote sensing and GIS: A case study of Prosopis juliflora in the UAE* [United Arab Emirates University, UAE]. https://scholarworks.uaeu.ac.ae/all_theses/512/

Donoghue, D. (2001). REMOTE SENSING AND IMAGE INTERPRETATION edited by Thomas M. Lillesand and Ralph W. Kiefer, John Wiley, New York, 2000. No. Of pages: 736. Price £29.95. ISBN 0 471 25515 7. *Earth Surface Processes and Landforms*, *26*(12), 1361–1361. https://doi.org/10.1002/esp.267

Fadda, E.H., Al Shebli, F., & Al Kabi, A. (2019). The use of remote sensing and GIS to study land use changes in Barka Wilaya, Oman. *Journal of Arts and Social Sciences*, *10*(1), 15-21. https://doi.org/10.24200/jass.vol10iss1pp15-20

Fan, X., Weng, Y., & Tao, J. (2016). Towards decadal soil salinity mapping using Landsat time series data. *International Journal of Applied Earth Observation and Geoinformation: ITC Journal*, *52*, 32–41. https://doi.org/10.1016/j.jag.2016.05.009

Foster, S., Pulido-Bosch, A., Vallejos, Á., Molina, L., Llop, A., & MacDonald, A.M. (2018). Impact of irrigated agriculture on groundwater-recharge salinity: a major sustainability concern in semi-arid regions. *Hydrogeology Journal*, *26*(8), 2781–2791. https://doi.org/10.1007/s10040-018-1830-2

Food and Agriculture Organization of the United Nations, (2009). Advances in the Assessment and Monitoring of Salinization and Status of Biosaline Agriculture: Report of an Expert Consultation Held in Dubai, United Arab Emirates, 26-29 November 2007. FAO, United Arab Emirates.

Gangjun, L. (1996). Land cover mapping in a Salinised Dryland farming area in southeastern Australia using Landsat TM data. *Geocarto International*, *11*(4), 47–59. https://doi.org/10.1080/10106049609354561

Ghazali, M.F., Wikantika, K., Harto, A.B., & Kondoh, A. (2020). Generating soil salinity, soil moisture, and soil pH from satellite imagery and its analysis. *Information Processing in Agriculture*, *7*(2), 294–306. https://doi.org/10.1016/j.inpa.2019.08.003

Goldshleger, N., Livne, I., Chudnovsky, A., & Ben-Dor, E. (2012). New results in integrating passive and active remote sensing methods to assess soil salinity. *Soil Science*, *177*(6), 392–401. https://doi.org/10.1097/ss.0b013e31824f167e

Gorji, T., Yıldırım, A., Sertel, E., & Tanık, A. (2019). Remote sensing approaches and mapping methods for monitoring soil salinity under different climate regimes. *International Journal of Environment and Geoinformatics*, *6*(1), 33–49. https://doi.org/10.30897/ijegeo.500452

Guo, X., Du, S., Guo, H., & Min, W. (2023). Long-term saline water drip irrigation alters soil physicochemical properties, bacterial community structure, and nitrogen transformations in cotton. *Applied Soil Ecology: A Section of Agriculture, Ecosystems & Environment*, *182*(19), 104719. https://doi.org/10.1016/j.apsoil.2022.104719

Hereher, M., Alghmdi, A., Mseddi, K., & El Kenawy, A. (2022). Remote sensing of vegetation prolonged drought at the salt playas of Hail–Saudi Arabia. *The Egyptian Journal of Remote Sensing and Space Science*, *25*(1), 135-145. https://doi.org/10.1016/j.ejrs.2022.01.006

Hereher, M., & El-Kenawy, A. (2022). Assessment of land degradation in northern Oman using geospatial techniques. *Earth Systems and Environment*, *6*(2), 469–482. https://doi.org/10.1007/s41748-021-00216-7

Huete, A.R., & Jackson, R.D. (1987). Suitability of spectral indices for evaluating vegetation characteristics on arid rangelands. *Remote Sensing of Environment*, *23*(2), 213-232. https://doi.org/10.1016/0034-4257(87)90038-1

Hussain, M.I., Shackleton, R., El-Keblawy, A., González, L., & Trigo, M.M. (2021). Impact of the invasive Prosopis juliflora on terrestrial ecosystems. *Sustainable Agriculture Reviews 52*, 223-278. https://doi.org/10.1007/978-3-030-73245-5_7

Hussain, N., Ai-Rawahy, S., Rabee, J., Al-Amri, M., & Causes, O. (2006). Genesis and Extent of Soil Salinity in the Sultanate of Oman. *Pakistan Journal Agriculture Science*, *43*, 1–10.

Ibnouf, M.A.O., & Abdelmagid, I.M. (1994). Oman water resources: Management, problems and policy alternatives. In *A Paper presented at the Second Gulf Water Conference," Water in the Gulf Region, Toward Integrated Management", Bahrain, held during the period* (pp. 19-31).

Ibrahim, M. (2016). Modeling soil salinity and mapping using spectral remote sensing data in the arid and semi-arid regions. *International Journal of Remote Sensing Application*, *6*(01), 76-82. https://doi.org/10.14355/ijrsa.2016.06.008

Ioka, M., & Koda, M. (1986). Performance of LANDSAT-5 TM data in land-cover classification. *International Journal of Remote Sensing*, *7*(12), 1715–1728. https://doi.org/10.1080/01431168608948963

Jarraya, H., & Benabdallah, S. (2020). Assessing aquifer water level and salinity for a managed artificial recharge site using reclaimed water. *Water*, *12*(2), 341-349. https://doi.org/10.3390/w12020341

Khadim, F.K., Su, H., Xu, L., & Tian, J. (2019). Soil salinity mapping in Everglades National Park using remote sensing techniques and vegetation salt tolerance. *Physics and Chemistry of the Earth (2002)*, *110*, 31–50. https://doi.org/10.1016/j.pce.2019.01.004

King, C., & Salem, B. (2012). A Socio-ecological investigation of options to manage groundwater degradation in the western desert, Egypt. *Ambio*, *41*(5), 490–503. https://doi.org/10.1007/s13280-012-0255-8

Kurbatova, A.I., Bouchhima, R.A., Grigorets, E.A., Tsymbarovich, P.R., & Ksibi, M. (2021). Methodology for mapping soil salinity and halophyte cover using remote sensing data in Kerkennah, Tunisia. *Euro-Mediterranean Journal for Environmental Integration*, *6*(2), 30-35. https://doi.org/10.1007/s41207-021-00257-4

Lemenkova, P. (2021). ISO Cluster classifier by ArcGIS for unsupervised classification of the Landsat TM image of Reykjavík. *Bulletin of Natural Sciences Research*, *11*(1), 29–37. https://doi.org/10.5937/bnsr11-30488

Mohammed, A.A., Al-Ghrairi, A.H.T., Al-zubidi, A.F., & Saeed, H.M. (2023). Unsupervised classification and analysis of Istanbul-Turkey satellite image utilizing remote sensing. *The Second International Scientific Conference (SISC2021): College of Science, Al-Nahrain University*. THE SECOND INTERNATIONAL SCIENTIFIC CONFERENCE (SISC2021): College of Science, Al-Nahrain University, Baghdad, Iraq. https://doi.org/10.1063/5.0118339

Morales-Gallegos, L.M., Martínez-Trinidad, T., Hernández-de la Rosa, P., Gómez-Guerrero, A., Alvarado-Rosales, D., & Saavedra-Romero, L. de L. (2023). Tree health condition in urban green areas assessed through crown indicator and vegetation indices. *Forests*, *14*(8), 1673. https://doi.org/10.3390/f14081673

Mouat, D.A., Mahin, G.G., & Lancaster, J. (1993). Remote sensing techniques in the analysis of change detection. *Geocarto International*, *8*(2), 39–50. https://doi.org/10.1080/10106049309354407

Muller, S.J., & van Niekerk, A. (2016). An evaluation of supervised classifiers for indirectly detecting salt-affected areas at the irrigation scheme level. *International Journal of Applied Earth Observation and Geoinformation: ITC Journal*, *49*, 138–150. https://doi.org/10.1016/j.jag.2016.02.005

Naifer, A., Al-Rawahy, S.A., & Zekri, S. (2011). Economic impact of salinity: The case of Al-batinah in Oman. *International Journal of Agricultural Research*, *6*(2), 134–142. https://doi.org/10.3923/ijar.2011.134.142

Neinavaz, E., Schlerf, M., Darvishzadeh, R., Gerhards, M., & Skidmore, A.K. (2021). Thermal infrared remote sensing of vegetation: Current status and perspectives. *International Journal of Applied Earth Observation and Geoinformation: ITC Journal*, *102*(15), 102415. https://doi.org/10.1016/j.jag.2021.102415

Nguyen, K.-A., Liou, Y.-A., Tran, H.-P., Hoang, P.-P., & Nguyen, T.-H. (2020). Soil salinity assessment by using near-infrared channel and Vegetation Soil Salinity Index derived from Landsat 8 OLI data: a case study in the Tra Vinh Province, Mekong Delta, Vietnam. *Progress in Earth and Planetary Science*, *7*(1), 21-30. https://doi.org/10.1186/s40645-019-0311-0

Oteman, B., Morris, E.P., Peralta, G., Bouma, T.J., & van der Wal, D. (2019). Using remote sensing to identify drivers behind spatial patterns in the bio-physical properties of a saltmarsh pioneer. *Remote Sensing*, *11*(5), 511. https://doi.org/10.3390/rs11050511

Prajapati, G.S., Rai, P.K., Mishra, V.N., Singh, P., & Shahi, A.P. (2021). Remote sensing-based assessment of waterlogging and soil salinity: A case study from Kerala, India. *Results in Geophysical Sciences*, *7*(24), 100024. https://doi.org/10.1016/j.ringps.2021.100024

Prudnikova, E., & Savin, I. (2018). Effect of open soil surface patterns on soil detectability based on optical remote sensing data. *The 2nd International Electronic Conference on Remote Sensing*, 2(7), 05-15. https://doi.org/10.3390/ecrs-2-05170

Prudnikova, E., Savin, I., Vindeker, G., Grubina, P., Shishkonakova, E., & Sharychev, D. (2019). Influence of soil background on the spectral reflectance of winter wheat crop canopy. *Remote Sensing*, *11*(16), 1932. https://doi.org/10.3390/rs11161932

Raj, R., Walker, J.P., Pingale, R., Nandan, R., Naik, B., & Jagarlapudi, A. (2021). Leaf area index estimation using top-of-canopy airborne RGB images. *International Journal of Applied Earth Observation and Geoinformation: ITC Journal*, *96*(10), 102282. https://doi.org/10.1016/j.jag.2020.102282

Ren, D., Wei, B., Xu, X., Engel, B., Li, G., Huang, Q., Xiong, Y., & Huang, G. (2019). Analyzing spatiotemporal characteristics of soil salinity in arid irrigated agro-ecosystems using integrated approaches. *Geoderma*, *356*(11), 113935. https://doi.org/10.1016/j.geoderma.2019.113935

Richards, J.A. (2022). Supervised Classification Techniques. In: Remote Sensing Digital Image Analysis. Springer, Cham. https://doi.org/10.1007/978-3-030-82327-6_8

Robertson, A.H.F., Searle, M.P., & Alison, C. (1990). *The geology and tectonics of the Oman region* (A. H. F. Robertson, etc., M. P. Searle, & A. C. Ries, Eds.). Geological Society, London. https://cir.nii.ac.jp/crid/1130000797568752384

Saxton, K.E., Rawls, W.J., Romberger, J.S., & Papendick, R.I. (1986). Estimating generalized soil-water characteristics from texture. *Soil Science Society of America Journal. Soil Science Society of America*, *50*(4), 1031–1036. https://doi.org/10.2136/sssaj1986.03615995005000040039x

Shahid, S.A. (2013). Developments in Soil Salinity Assessment, Modeling, Mapping, and Monitoring from Regional to Submicroscopic Scales. In: Shahid, S., Abdelfattah, M., Taha, F. (eds) Developments in Soil Salinity Assessment and Reclamation. Springer, Dordrecht, Netherlands. https://doi.org/10.1007/978-94-007-5684-7_1

Shahid, S.A., Mahmoud, A., Samira, A.S., Omar, H., Harahsheh, Y., & Othman, H. (2010). Mapping and Monitoring of Soil Salinization Remote Sensing, GIS, Modeling, Electromagnetic Induction, and Conventional Methods-Case Studies. *Proceedings of the International Conference on Soils and Groundwater Salinization in Arid Countries*, *59(1),* 59-98.

Siebert, S., Nagieb, M., & Buerkert, A. (2007). Climate and irrigation water use of a mountain oasis in northern Oman. *Agricultural Water Management*, *89*(1–2), 1–14. https://doi.org/10.1016/j.agwat.2006.11.004

Smanov, Z.M., Laiskhanov, S.U., Poshanov, M.N., Abikbayev, Y.R., Duisekov, S.N., & Tulegenov, Y.A. (2023). Mapping of cornfield soil salinity in arid and semi-arid regions. *Journal of Ecological Engineering*, *24*(1), 491-497.

Suleymanov, A., Gabbasova, I., Komissarov, M., Suleymanov, R., Garipov, T., Tuktarova, I., & Belan, L. (2023). Random Forest Modeling of Soil Properties in Saline Semi-Arid Areas. *Agriculture*, *13*(5), 23-45. https://doi.org/10.3390/agriculture13050976

Taghizadeh-Mehrjardi, R., Schmidt, K., Toomanian, N., Heung, B., Behrens, T., Mosavi, A., Band, S., Amirian-Chakan, A., Fathabadi, A., & Scholten, T. (2021). Improving the spatial prediction of soil salinity in arid regions using wavelet transformation and support vector regression models. *Geoderma*, *383*(01), 114793. https://doi.org/10.1016/j.geoderma.2020.114793

Taunk, K., De, S., Verma, S., & Swetapadma, A. (2019). A brief review of nearest neighbor algorithm for learning and classification. 2019 International Conference on Intelligent Computing and Control Systems (ICCS). 2019 International Conference on Intelligent Computing and Control Systems (ICCS), Madurai, India. https://doi.org/10.1109/ iccs45141.2019.9065747

Vani, V., & Mandla, V.R. (2017). Comparative study of ndvi and Savi vegetation indices in Anantapur district semi-arid areas. *International Journal of Civil Engineering and Technology*, *8*(4), 559–566. https://iaeme.com/MasterAdmin/Journal_uploads/IJCIET/VOLUME_8_ISSUE_4/IJCIET_08_04_063.pdf

Vimala, R., Marimuthu, A., Venkateswaran, S., & Poongodi, R. (2020). Unsupervised ISODATA algorithm classification used in the Landsat image for predicting the expansion of Salem urban, Tamil Nadu. *Indian Journal of Science and Technology*, *13*(16), 1619–1629. https://doi.org/10.17485/ijst/v13i16.271

Wen, X., Lu, J., Wu, J., Lin, Y., & Luo, Y. (2019). Influence of coastal groundwater salinization on the distribution and risks of heavy metals. *The Science of the Total Environment*, *652*, 267–277. https://doi.org/10.1016/j.scitotenv.2018.10.250

Wu, B., Zhang, M., Zeng, H., Tian, F., Potgieter, A.B., Qin, X., Yan, N., Chang, S., Zhao, Y., Dong, Q., Boken, V., Plotnikov, D., Guo, H., Wu, F., Zhao, H., Deronde, B., Tits, L., & Loupian, E. (2023). Challenges and opportunities in remote sensing-based crop monitoring: a review. *National Science Review*, *10*(4), 290-297. https://doi.org/10.1093/nsr/nwac290

Yu, Z., Di, L., Yang, R., Tang, J., Lin, L., Zhang, C., & Sun, Z. (2019). Selection of landsat 8 OLI band combinations for land use and land cover classification. In *2019 8th International Conference on Agro-Geoinformatics (Agro-Geoinformatics)* (pp. 1-5), IEEE, Istanbul, Turkey. https://doi.org/10.1109/agro-geoinformatics.2019.8820595

Zhang, T.-T., Zeng, S.-L., Gao, Y., Ouyang, Z.-T., Li, B., Fang, C.-M., & Zhao, B. (2011). Using hyperspectral vegetation indices as a proxy to monitor soil salinity. *Ecological Indicators*, *11*(6), 1552–1562. https://doi.org/10.1016/j.ecolind.2011.03.025

Zhou, H., Zhou, G., Song, X., & He, Q. (2022). Dynamic characteristics of canopy and vegetation water content during an entire maize growing season about spectral-based indices. *Remote Sensing*, *14*(3), 584. https://doi.org/10.3390/rs14030584